RSC Advances

PAPER

View Article Online
View Journal | View Issue

Published on 02 February 2015. Downloaded by Michigan State University on 21/01/2016 23:06:36.

Cite this: *RSC Adv.*, 2015, **5**, 19647

Effect of $CaZrO_3$ on phase structure and electrical properties of KNN-based lead-free ceramics

Yang Zhang,[a] Lingyu Li,[a] Wangfeng Bai,[a] Bo Shen,[a] Jiwei Zhai*[a] and Bo Li[b]

Received 16th December 2014
Accepted 28th January 2015

DOI: 10.1039/c4ra16506c

www.rsc.org/advances

$(1-x)[0.93(K_{0.5}Na_{0.5})NbO_3-0.07LiNbO_3]-xCaZrO_3$ (KNN–LN–*x*CZ) lead-free piezoelectric ceramics have been prepared by the conventional solid state reaction method and investigated to differentiate the effects of polymorphic phase transition. The crystal structure of the ceramics changed from orthorhombic to tetragonal at $x \geq 0.04$, and then both the orthorhombic and tetragonal phases coexisted in the region of $0.04 < x < 0.08$ composition, and the orthorhombic–tetragonal phase transition temperature was modified to around room temperature. Remarkably, piezoelectric and ferroelectric properties have been obtained for KNN–LN–*x*CZ ternary system with $x = 0.04$, in which the piezoelectric parameter of d^*_{33} was 320 pm V^{-1} with Curie temperature $T_c = 350$ °C, strain level = 0.16% at 50 kV cm^{-1} and remnant polarization $P_r = 27.2$ μC cm^{-2}.

1. Introduction

PZT-based piezoelectric ceramics have been widely utilized over several decades due to their superior piezoelectric properties.[1,2] However, the high toxicity of lead oxide has caused serious environmental problems. Therefore, there is a great need to develop lead-free piezoelectric ceramics with good piezoelectric properties to replace these lead-based ceramics in various applications.[3–5] Many lead-free ferroelectric materials, such as barium titanate (BT),[6,7] potassium niobate (KN),[8] potassium sodium niobate (KNN),[9–21] potassium tantalate niobate (KTN)[22–25] and bismuth sodium titanate (BNT),[26–28] have been investigated. Among all the lead-free materials, $K_{0.5}Na_{0.5}NbO_3$ (KNN), the solid solution of ferroelectric $KNbO_3$ and antiferroelectric $NaNbO_3$, has been studied extensively. This material is considered to be one of the most promising candidates for lead-free piezoelectric ceramics due to its high Curie temperature, outstanding piezoelectric and ferroelectric properties, and large electromechanical coupling coefficient. Moreover, it also possesses better environmental compatibility than other lead-free piezoelectric ceramics; these superior piezoelectric properties are attributed to its orthorhombic–tetragonal polymorphic phase transition (PPT) around room temperature. These superior properties are considered to be closely associated with the coexistence of these phases, which is similar to the morphotropic phase boundary (MPB)—a phase boundary that is a narrow composition region with an orthorhombic or monoclinic phase that separates rhombohedral and tetragonal phases in solid solutions—found in widely used PZT-based ceramics.[29,30]

However, in contrast to the classical behaviors of nearly temperature-independent MPB, strong piezoelectric temperature dependence is usually observed in KNN-based ceramics with high piezoelectric properties.[22] It was reported that a PPT existed in $(1-x)(K_{0.5}Na_{0.5})NbO_3-x(LiNbO_3)$ at about 5–7 mol% of $LiNbO_3$, which exhibited excellent piezoelectric properties and high Curie temperature.[31] Yao *et al.*[32] reported $CaZrO_3$ modified KNN-based ceramics, which could reduce lattice distortion and the coexistence of orthorhombic and tetragonal phases.

In this work, KNN–LN–*x*CZ ceramics were prepared by a conventional solid state reaction route, and the influences of $CaZrO_3$ on the crystal structure and electrical properties of the ceramics were investigated. $LiNbO_3$ was expected to enhance the piezoelectric properties of KNN ceramics. $CaZrO_3$ was proposed to modify the KNN-based systems, improving the temperature dependence of the KNN ceramics.

2. Experimental procedure

KNN–LN–*x*CZ ceramics with $x = 0$, 0.02, 0.04, 0.06, 0.08 and 0.10 were prepared by a conventional solid-state reaction route. The raw materials of Na_2CO_3 (99.95%), K_2CO_3 (99%), Li_2CO_3 (99%), Nb_2O_5 (99.9%), ZrO_2 (99%) and $CaCO_3$ (99%) powders were mixed by planetary mill for 24 h in ethanol. This mixture was calcined at 850 °C for 6 h. After calcination, the powder was crushed and ball-milled again for 24 h. Then, the dried powder was mixed with polyvinyl alcohol (PVA) binder solution and pressed into pellets with a diameter of 10 mm, and sintered at

[a]*Key Laboratory of Advanced Civil Engineering Materials of Ministry of Education, Functional Materials Research Laboratory, School of Materials Science & Engineering, Tongji University, 4800 Caoan Road, Shanghai 201804, China. E-mail: apzhai@tongji.edu.cn*

[b]*Department of Orthopaedics, Yueyang Hospital of Integrated Chinese Medicine and Western Medicine, Shanghai University of Traditional Chinese Medicine, 110 Ganhe Road, Shanghai 200437, China*

Published on 02 February 2015. Downloaded by Michigan State University on 21/01/2016 23:06:36.

1120 °C to 1180 °C for 2 h in an ambient atmosphere. The phase structure of the samples was examined by XRD (Bruker D8 Advance, Karlsruhe, Germany) with CuKα radiation. The microstructures of samples were characterized using scanning electron microscopy (SEM) (JSM, EMP-800; JEOL, Tokyo, Japan). To study their electrical properties, the samples were polished and painted with silver pastes on both the sides and then fired at 600 °C for 30 min. The temperature dependence of the dielectric constant and loss of the samples were measured with a high-precision LCR meter (Agilent E4980A, Agilent, Palo Alto, CA). The FE hysteresis loops and strain curves of the samples were measured at 10 Hz by a Radiant Precision Workstation (USA) connected with a Miniature Plane-mirror Interferometer and the accessory Laser Interferometric Vibrometer (Germany). The samples were polarized in silicone oil under 40 kV cm^{-1} at room temperature for 30 min. The piezoelectric constant d_{33} was measured using a quasi-static d_{33} meter (IACAS ZJ-6A).

3. Results and discussion

The phase structures of KNN–LN–*x*CZ ceramics were analyzed by combining XRD patterns and ε_r *vs.* T, and the detailed analysis is listed in the subsequent sections. Fig. 1(a) shows that all the ceramics have a pure perovskite structure without any secondary phase, confirming that the ceramics are complete solid solutions. To identify the phase transition, the expanded XRD patterns of the ceramics in the range from 44° to 47° were obtained and are shown in Fig. 1(b). The diffraction peak (002) gradually rises with increasing x content, and then the two diffraction peaks, namely, (200) and (002), start to merge together at $x \geq 0.08$. The transition of the orthorhombic phase to the tetragonal phase occurs at the compositions $x \geq 0.04$. Thus, the orthorhombic and tetragonal ferroelectric phases of the ceramics coexisted in the composition range of $0.04 \leq x \leq 0.08$ at room temperature. The phase boundary of an orthorhombic phase transforming to a tetragonal phase is denoted as PPT. For this work, the PPT composition region is $0.04 \leq x \leq 0.08$; therefore, investigation into the piezoelectric and ferroelectric properties will be focused on the composition of $0.04 \leq x \leq 0.08$.

KNN-based materials have different phase transition temperatures;[33] KNN undergoes the following structural phase transformation sequence: ferroelectric rhombohedral (R) $\xrightarrow{\sim -150\ ^\circ C}$ ferroelectric orthorhombic (O) $\xrightarrow{\sim 210\ ^\circ C}$ ferroelectric tetragonal (T) $\xrightarrow{\sim 415\ ^\circ C}$ paraelectric cubic (C). The dielectric peak of T_C can be clearly observed, and T_C value is indeed dependent on the $CaZrO_3$ content. As shown in Fig. 2, the maximum dielectric constant located at the T_C initially increases and then decreases dramatically. The composition with $x = 0$ undergoes the cubic–tetragonal phase transition at 447 °C (T_C) and the tetragonal–orthorhombic phase transition at 114 °C ($T_{O\rightarrow T}$). It can be seen from Fig. 2 that the $T_{O\rightarrow T}$ phase is moving towards room temperature. On the basis of these results, it can be concluded that these compositions should have an orthorhombic structure at room temperature. Based on the abovementioned observations, phase diagrams were constructed for KNN–LN–*x*CZ ceramics, as shown in Fig. 3. Three phase regions, namely, orthorhombic, tetragonal and cubic phases, are divided by T_C and $T_{O\rightarrow T}$. Both T_C and $T_{O\rightarrow T}$ decreased with increasing x, but T_C dropped dramatically, whereas $T_{O\rightarrow T}$ phase decreased towards room temperature from 114 °C to 25 °C. Moreover, d_{33} values measured at room temperature are also shown in Fig. 3. With $CaZrO_3$ substitution, d_{33} increases to 202 pC N^{-1} at $x = 0.04$, and then decreases with further substitution. The enhanced piezoelectric behavior of KNN–LN–*x*CZ ceramics cannot be simply attributed to a particular content; the new phase boundary in KNN–LN–*x*CZ ceramics with $T_{O\rightarrow T}$ phase towards room temperature acts as a dominant factor, and the coexistence of two phases is still a necessary condition for high d_{33} values.

The SEM images of the KNN–LN–*x*CZ ceramics are shown in Fig. 4. For the ceramic with $x = 0$, the grain size is from 2.5 to 3.0 μm. It is noted that the grain size decreases dramatically as x increases and more uniform grains are observed, as shown in the Fig. 4(c) and (d). This result indicates that a low content of

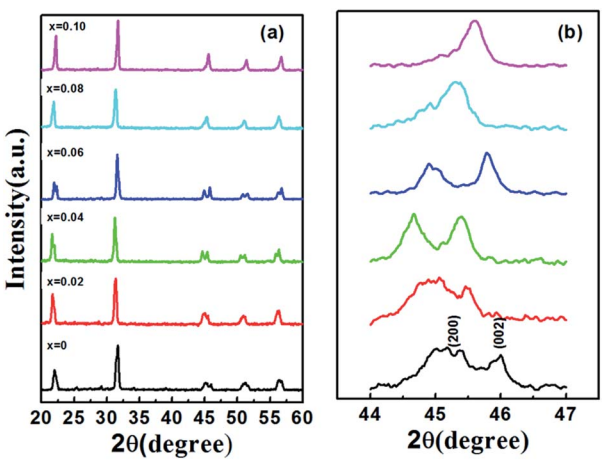

Fig. 1 XRD patterns of the KNN–LN–*x*CZ ceramics in the 2θ range of (a) 20–60° and (b) 44–47°.

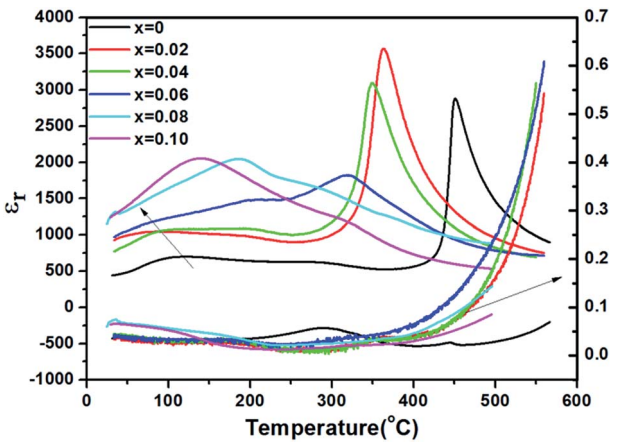

Fig. 2 Temperature dependence of the dielectric constant and dielectric loss of the KNN–LN–*x*CZ ceramics measured at 10 kHz in the temperature range from room temperature to 550 °C.

This journal is © The Royal Society of Chemistry 2015

Published on 02 February 2015. Downloaded by Michigan State University on 21/01/2016 23:06:36.

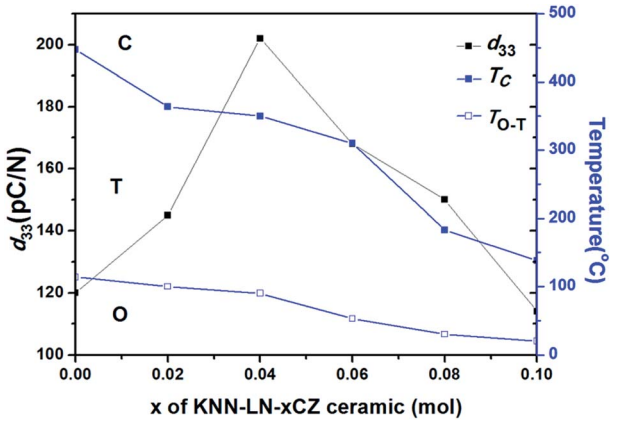

Fig. 3 Phase diagrams (T_C and $T_{O\rightarrow T}$) of the KNN–LN–xCZ ceramics showing the difference caused by $CaZrO_3$ substitution; d_{33} is also shown at room temperature.

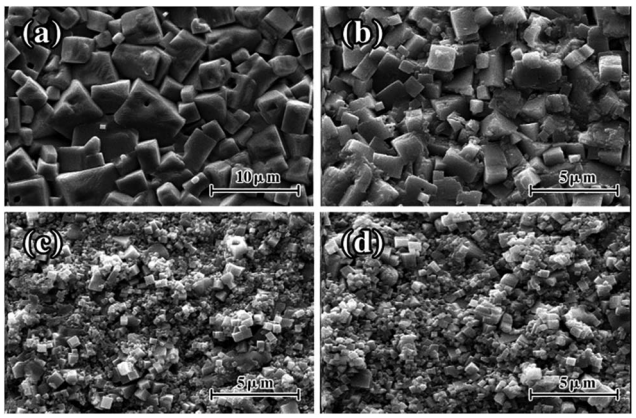

Fig. 4 SEM images of the ceramics with (a) $x = 0$, (b) $x = 0.04$, (c) $x = 0.06$, and (d) $x = 0.08$ sintered at 1160 °C for 2 h.

$CaZrO_3$ can efficiently diffuse into the KNN lattices to change the phase structure; however, if x is higher, some of the $CaZrO_3$ will inhibit the grain growth.

The variations of the remanent polarization P_r and coercive field E_c with $x = 0$, 0.04, 0.06 and 0.08 for the ceramics are shown in Fig. 5. All the KNN–LN–xCZ ceramics exhibit a well-saturated P–E loop under an electric field of about 60 kV cm^{-1}. The remanent polarization of $P_r = 27.2$ μC cm^{-2} was obtained at $x = 0.04$, which is higher than the others. The high P_r is probably attributed to both the domain switching and non-180° domain contribution,[6,26] as well as the decrease of $T_{O\rightarrow T}$ phase towards room temperature; moreover, the polarization direction can be easily rotated by external electric fields.

It can be observed from Fig. 6(a) that all the samples exhibit typical butterfly-shape strain curves; apparently, for $x = 0.04$, the total strain of 0.16% and a larger negative strain of 0.025% were obtained at an electric field of 50 kV cm^{-1}, which is typical for an FE material. With the increase of $CaZrO_3$ content, the strain curves show a deviation from the typical FE behavior; as a result, the strain decreases to 0.13% for $x = 0.08$ with little

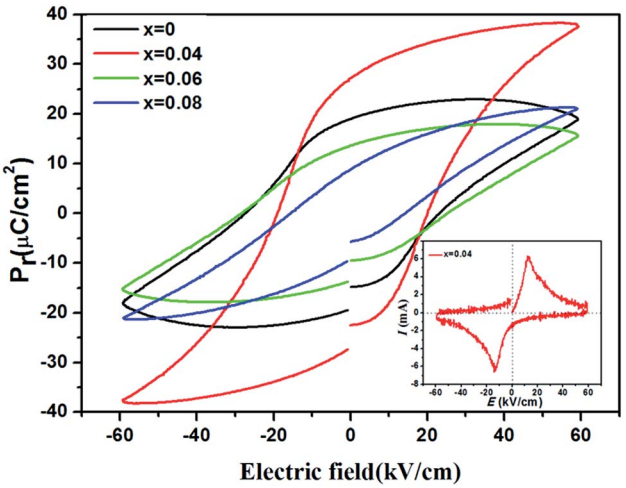

Fig. 5 P–E hysteresis loops of the KNN–LN–xCZ ceramics (inset shows I–E curves) measured at 10 Hz.

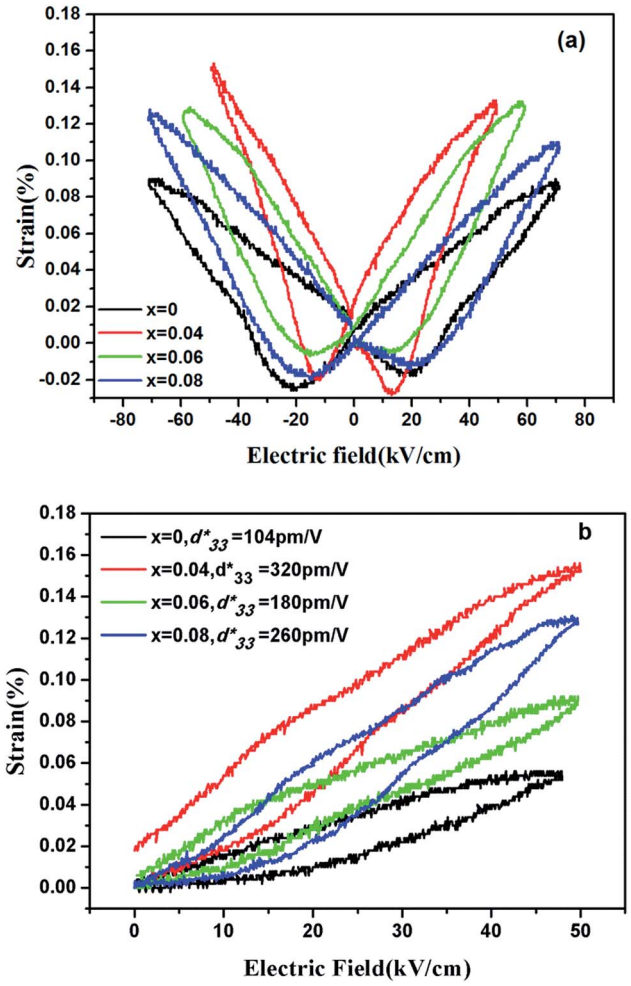

Fig. 6 S–E curves of the KNN–LN–xCZ ceramics measured at 10 Hz and room temperature for (a) bipolar strain and (b) unipolar strain.

Published on 02 February 2015. Downloaded by Michigan State University on 21/01/2016 23:06:36.

Table 1 Piezoelectric and dielectric properties of the KNN–LN–xCZ ceramics with $x = 0$, $x = 0.04$, $x = 0.06$, $x = 0.08$

	d_{33} (pC N^{-1})	d^*_{33} (pm V^{-1})	T_c (°C)	tan δ (%)	P_r (μC cm^{-2})	ε_r (25 °C)	Strain (%)
$x = 0$	120	104	447	0.036	18.8	2880	0.05
$x = 0.04$	202	320	350	0.038	27.2	3083	0.16
$x = 0.06$	168	180	310	0.045	14.3	1806	0.09
$x = 0.08$	150	260	183	0.07	8.7	2043	0.13

negative strain. This can imply that a small negative strain promotes the potential for a material to display a large strain response. Moreover, the high strain value could be from the non-180° domain contribution. As can be seen from Fig. 6(b), a larger strain of 0.16% was obtained at $x = 0.04$, which is similar to that in Fig. 6(a). The corresponding dynamic piezoelectric coefficient, $d^*_{33} = S_{max}/E_{max}$, gives a maximum value of 320 pm V^{-1} at $x = 0.04$ compared with the reported values for other KNN-based ceramics, such as 310 pm V^{-1} for $K_{0.485}Na_{0.485}Li_{0.03}Nb_{0.8}Ta_{0.2}O_3$ (ref. 34) and 252 pm V^{-1} for KNN modified with $LiNbO_3$,[35] revealing that KNN–LN–xCZ ceramic has a superior piezoelectric property at the phase boundary. When $CaZrO_3$ was added, Ca^{2+} and Zr^{4+} were introduced into A-site and B-site, respectively, which increased the deviation displacement because the radius of Ca^{2+} ($R = 1.34$ Å, CN = 12)[36,37] is smaller than that of K^+ ($R = 1.64$ Å, CN = 12) and Na^+ ($R = 1.39$ Å, CN = 12), whereas the radius of Zr^{4+} (R = 0.72 Å, CN = 6) is larger than that of Nb^{5+} ($R = 0.64$ Å, CN = 6).[38] The increase of the deviation displacement gives rise to a local polar moment, leading to the formation of more macropolar domains at room temperature. Moreover, with the replacement of Ca^{2+} and Zr^{4+} at A-site and B-site, respectively, the ionic radius becomes smaller and induces a lattice distortion at phase boundary. As observed in Fig. 1(b), diffraction peak positions shift towards the lower angle due to the substitution of $CaZrO_3$ until $x = 0.04$ mol, and then diffraction peak positions shift towards the higher angle with increasing $CaZrO_3$ content. Lattice distortion results in shifts of diffraction peak positions; therefore, $x = 0.04$ can be considered as a transition point, which is in the region of PPT, as reported previously.[39] d_{33} at $T_{O\rightarrow T}$ is affected by the coexistence of two phases with more polarization directions; lattice distortion also affects d_{33}. As the distortion becomes smaller towards the PPT, relatively less strain in domain switching is induced during poling, and subsequently a higher d_{33} is obtained because of the better alignment of domains.

As discussed above, the material has a good performance at $x = 0.04$; moreover, the properties of KNN–LN–xCZ ceramics with $x = 0$, $x = 0.04$, $x = 0.06$ and $x = 0.08$ are summarized in Table 1. Obviously, the KNN–LN–xCZ ceramics at $x = 0.04$ exhibited outstanding performance with piezoelectric constant $d_{33} = 202$ pC N^{-1}, $d^*_{33} = 320$ pm V^{-1}, remanent polarization $P_r = 27.2$ μC cm^{-2} and maximum strain level of 0.16% at an electric field of 50 kV cm^{-1}, which were superior to those of others. These good performances suggested that the 0.96 KNN–LN–0.04CZ ceramic is a promising lead-free piezoelectric material.

4. Conclusions

Lead-free $(1 - x)[0.93(K_{0.5}Na_{0.5})NbO_3–0.07LiNbO_3]–xCaZrO_3$ ternary system piezoelectric ceramics was prepared by a conventional ceramic technology, and their phase structure, microstructures and electrical properties were investigated in detail. The crystal structure of KNN–LN–xCZ ceramics was changed from orthorhombic to tetragonal at $x \geq 0.04$, and then both the orthorhombic and tetragonal phases coexisted at $0.04 < x < 0.08$, which were converted to a pure tetragonal structure at $x > 0.08$. The Curie temperature decreased with increasing $CaZrO_3$ content. At the phase boundary, the maximum value of $d_{33} = 202$ pC N^{-1} and $d^*_{33} = 320$ pm V^{-1} were obtained at $x = 0.04$ with Curie temperature $T_c = 350$ °C, strain levels = 0.16% at 50 kV cm^{-1} and remanent polarization $P_r = 27.2$ μC cm^{-2}. The polymorphic phase transition between the orthorhombic and tetragonal phases played a very important role in the enhancement of the piezoelectric properties of KNN–LN–xCZ ceramics. These good performances suggested that the KNN–LN–xCZ ceramic is a promising lead-free piezoelectric material.

Acknowledgements

The authors would like to acknowledge the National Natural Science Foundation of China under Grant no. 51372171, 51332003 and the Shanghai Municipal Natural Science Foundation under Grant no. 12ZR1434600.

Notes and references

1 G. H. Haertling, *J. Am. Ceram. Soc.*, 1999, **82**, 797–818.
2 D. E. Cox, B. Noheda, G. Shirane, Y. Uesu, K. Fujishiro and Y. Yamada, *Appl. Phys. Lett.*, 2001, **79**, 400.
3 D. Maurya, A. Pramamick and M. Feygenson, *et al.*, *J. Mater. Chem. C*, 2014, **2**, 8423–8431.
4 Y. Saito, H. Takao, T. Tani, T. Nonoyama, K. Takatori, T. Homma, T. Nagaya and M. Nakamura, *Nature*, 2004, **432**, 84–87.
5 P. Gu Kang, B. Kil Yun and K. Dong Sung, *et al.*, *RSC Adv.*, 2014, **4**, 29799.
6 G. Viola, T. Saunders, X. Wei, K. B. Chong, H. Luo, M. J. Reece and H. Yan, *J. Adv. Dielectr.*, 2013, **3**, 1350007.
7 D. Maurya, Y. Zhou, Y. Yan and S. Priya, *J. Mater. Chem. C*, 2013, **1**, 2102–2111.
8 E. Aksel and J. L. Jones, *Sensors*, 2010, **10**, 1935–1954.
9 J. G. Wu, *RSC Adv.*, 2014, **4**, 53490.
10 F. Z. Yao, Q. Yu, K. Wang, Q. Li and J. F. Li, *RSC Adv.*, 2014, **4**, 20062.
11 J.-F. Li, Y. Zhen, B.-P. Zhang and L.-M. Zhang, *Ceram. Int.*, 2008, **34**, 783–786.
12 H. Du, F. Tang, F. Luo, D. Zhu, S. Qu, Z. Pei and W. Zhou, *Mater. Res. Bull.*, 2007, **42**, 1594–1601.
13 Y. Zhen and J. F. Li, *J. Am. Ceram. Soc.*, 2006, **89**, 3669–3675.
14 Z. Shen, Y. Li and L. Jiang, *J. Mater. Sci.: Mater. Electron.*, 2011, **22**, 1071–1075.
15 C. Kiang Ivan Tan and K. Yao, *J. Am. Ceram. Soc.*, 2011, **94**, 776–781.

 This journal is © The Royal Society of Chemistry 2015

Published on 02 February 2015. Downloaded by Michigan State University on 21/01/2016 23:06:36.

16 B. Zhang, J. Wu and X. Cheng, *et al.*, *ACS Appl. Mater. Interfaces*, 2013, **5**, 7718–7725.
17 M. Matsubara, K. Kikuta and S. Hirano, *Jpn. J. Appl. Phys.*, 2005, **44**, 6618–6623.
18 Y. Guo, K. Kakimoto and H. Ohsato, *Appl. Phys. Lett.*, 2004, **85**, 4121–4123.
19 P. Kumar and P. Palei, *Ceram. Int.*, 2010, **36**, 1725–1729.
20 S. J. Zhang, R. Xia, T. R. Shrout, G. Z. Zang and J. F. Wang, *J. Appl. Phys.*, 2006, **100**, 104108.
21 J.-F. Li, K. Wang, B.-P. Zhang and L. M. Zhang, *J. Am. Ceram. Soc.*, 2006, **89**, 706–709.
22 E. Hollenstein, M. Davis, D. Damjanovic and N. Setter, *Appl. Phys. Lett.*, 2005, **87**, 182905.
23 J. L. Zhang, X. J. Zong, L. Wu, Y. Gao, P. Zheng and S. F. Shao, *Appl. Phys. Lett.*, 2009, **95**, 022909.
24 T. A. Skidmore, T. P. Comyn and S. J. Milne, *Appl. Phys. Lett.*, 2009, **94**, 222902.
25 Y. Chang, Z. Yang, D. Ma, Z. Liu and Z. Wang, *J. Appl. Phys.*, 2009, **105**, 054101.
26 H. Yan, F. Inam and G. Viola, *et al.*, *J. Adv. Dielectr.*, 2011, **1**, 107–118.
27 D. Maurya, A. Kumar and V. Petkov, *et al.*, *RSC Adv.*, 2014, **4**, 1283–1292.
28 D. Maurya, M. Murayama, A. Pramanick, W. T. Reynolds Jr, K. An and S. Priya, *J. Appl. Phys.*, 2013, **113**, 114101.
29 D. E. Cox, B. Noheda, G. Shirane, Y. Uesu, K. Fujishiro and Y. Yamada, *Appl. Phys. Lett.*, 2001, **79**, 400.
30 T. Huang, D. Q. Xiao, C. Liu, F. X. Li, B. Wu, J. G. Wu and J. G. Zhu, *Ceram. Int.*, 2014, **40**, 2731–2735.
31 Y. Guo, K. I. Kakimoto and H. Ohsato, *Appl. Phys. Lett.*, 2004, **85**, 4121–4123.
32 F. Z. Yao, E. A. Patterson, K. Wang, W. Jo, J. Rödel and J. F. Li, *Appl. Phys. Lett.*, 2014, **104**, 242912.
33 W. Ge, J. Li and D. Viehland, *Phys. Rev. B: Condens. Matter Mater. Phys.*, 2011, **83**, 224110.
34 E. Hollenstein, M. Davis, D. Damjanovic and N. Setter, *Appl. Phys. Lett.*, 2005, **87**, 182905–182908.
35 E. Li, R. Suzuki, T. Hoshina, H. Takeda and T. Tsurumi, *Appl. Phys. Lett.*, 2009, **94**, 132903–132905.
36 H. Du, W. Zhou and D. Zhu, *et al.*, *J. Am. Ceram. Soc.*, 2008, **91**, 2903–2909.
37 R. D. Shannon, *Acta Crystallogr., Sect. A: Cryst. Phys., Diffr., Theor. Gen. Crystallogr.*, 1976, **32**, 751.
38 V. Bobnar, J. Bernard and M. Kosec, *Appl. Phys. Lett.*, 2004, **85**, 994.
39 Y. S. Sung, J. M. Kim, J. H. Cho, T. K. Song, M. H. Kim and T. G. Park, *Appl. Phys. Lett.*, 2010, **96**, 202901.